

Joint inversion of P- and SV-wave traveltimes to estimate anisotropy: a CFP approach

Robert J. Ferguson, Jackson School of Geosciences, Department of Geological Sciences, University of Texas at Austin, and Mrinal Sen, Jackson School of Geosciences, Institute for Geophysics, University of Texas at Austin

SUMMARY

A method is presented to estimate the elastic parameters and thickness of a locally homogeneous medium using compressional-wave (P-wave) and vertically-polarized-shear wave (SV-wave) data. This method is a "layer-stripping" technique, and uses many aspects of common-focal-point technology. For each layer, a focusing operator and a CFP gather are computed using estimated-elastic parameters. Assuming local homogeneity, the resulting differential time shifts (DTSs) represent error in the elastic parameters and error in thickness. In the $\tau-p$ domain, DTSs $\Delta\tau$ are shown to link error in layer-thickness z and vertical slowness q , to horizontal slowness p . Series expansion is used to linearize $\Delta\tau$ with respect to error in the elastic parameters and thickness, and least-squares inversion is used to estimate error for use in updating the model.

For stability, joint inversion P- and SV-data is employed and, as pure SV-data are relatively rare, the use of mode-converted (PSV) data to represent SV in the joint inversion is suggested. Analytic and synthetic examples are used to demonstrate the practicality of this inversion and its robustness in the presence of noise.

INTRODUCTION

Common Focal Point (CFP) technology (Berkhout and Verschuur, 2001) is a useful tool in exploration seismology. CFPs are selected for reflectors of interest, and operators are used to back propagate the reflection data to the CFPs. CFP gathers are then cross-correlated with their corresponding focusing operators (computed by forward propagating models of the seismic sources). For operators that exactly mimic wave propagation from the source and receiver locations to the CFP, energy corresponding to specular reflection aligns at zero-lag on the CFP gather. The amplitude of this energy is a measure of the reflectivity at the CFP location, and can be analyzed as such, or summed into an average reflectivity for imaging (de Bruin et al., 1990). Misalignment, or differential time shift (DTS), is the result of error in estimating the heterogeneity and anisotropy of the medium above. In strict adherence to the CFP method, DTSs are used to update vertical slowness q such that, upon subsequent analysis, alignment is achieved and optimal reflectivity is obtained.

A departure from the CFP method uses DTS measurements to estimate velocity heterogeneity for isotropic media where a constrained parametric inversion is used to deduce lateral velocity variation (Kabir and Verschuur, 2000). Though this method may not improve the resulting image relative to CFP imaging, it has value in providing estimates of velocity intermediate to imaging.

In anisotropic media, estimating the elastic parameters of the medium above the CFP can be considered by picking DTSs in the $\tau-p$ domain. DTSs ($\Delta\tau$) in $\tau-p$ provide a relationship between horizontal slowness p , error in vertical slowness q , and error in layer thickness z . Here, an analytic expression for $\Delta\tau$ is derived using a Taylor series expansion of q in the initial values of anisotropic parameters. Linearization provides a simple relationship between the DTS and errors in the anisotropic parameters suitable for linear inversion.

For stability, joint inversion of P-wave and S-wave data is preferred to inversion of P-wave data alone. Though recordings of SH- and SV-data are uncommon in reflection seismology, recording the converted SV-mode (PSV) is increasingly common, and here the PSV-mode is suggested as being suitable for use in the joint inversion in stead of a pure SV-mode.

Analytic and synthetic experiments are presented here to show convergence of this inversion method for VTI media, and to demonstrate the methodology. In the presence of random noise, the joint inversion is shown to be quite robust, and converges in a few iterations. As noise increases, convergence requires more iterations, and the parameter ϵ of (Thomsen, 1986) is found to converge most slowly.

THEORY

For horizontal slowness p , and temporal frequency ω , the plane-wave-reflection coefficient R for a reflector at depth z is the quotient of incident wavefield $\phi^I(z)$ and reflected wavefield $\phi^R(z)$

$$R(p, \omega, z) = \frac{\phi^R(p, \omega, z)}{\phi^I(p, \omega, z)}, \quad (1)$$

where, for general wavefield ϕ ,

$$\phi(p, \omega) = \int \psi(x, \omega) e^{i\omega px} dx, \quad (2)$$

with

$$\psi(x, \omega) = \frac{1}{2\pi} \int \psi(x, t) e^{-i\omega t} dt. \quad (3)$$

For homogeneous media, the required wavefields at z can be computed by phase shifting known wavefields from reference level $z=0$ (Gazdag, 1978). To obtain $\phi^I(z)$, phase shift source-wavefield $\phi^I(z=0)$ from $z=0$ to z using an estimate \tilde{q} of true-vertical slowness q

$$\phi^I(p, \omega, z) = \phi^I(p, \omega, z=0) e^{iz\omega\tilde{q}(p)}. \quad (4)$$

To obtain $\phi^R(z)$, reverse-phase shift reflected-wavefield $\phi^R(z=0)$

$$\phi^R(p, \omega, z) = \phi^R(p, \omega, z=0) e^{-iz\omega\tilde{q}(p)}, \quad (5)$$

where the negative sign in the phase term causes a reverse-phase shift relative to equation (4).

Wavefield $\phi^R(z=0)$ results from phase shifting $\phi^I(z=0)$ from $z=0$ to z , then scaling it by $R(z)$, and then phase shifting it back to $z=0$, so $\phi^R(z=0)$ can be written as a function of source wavefield $\phi^I(z=0)$

$$\phi^R(p, \omega, z=0) = \phi^I(p, \omega, z=0) e^{iz\omega q(p)} R(p, \omega, z) e^{iz\omega q(p)}. \quad (6)$$

Substitution of equation (6) into equation (5) gives $\phi^R(p, \omega, z)$ in terms of $\phi^I(z=0)$

$$\phi^R(p, \omega, z) = \phi^I(p, \omega, z=0) e^{2iz\omega q(p)} R(p, \omega, z) e^{-iz\omega\tilde{q}(p)}. \quad (7)$$

For $\tilde{q} \neq q$, an approximate-reflectivity \tilde{R} using equations (1), (4), and (7) is

$$\tilde{R}(p, \omega, z) = e^{i\omega\Delta\tau(p)} R(p, \omega, z), \quad (8)$$

— a phase-shifted version of true-reflectivity R , where travel-time error $\Delta\tau$ is given by

$$\Delta\tau(p) = 2z[q(p) - \tilde{q}(p)]. \quad (9)$$

Travel-time errors $\Delta\tau$ are the DTSs on the (p, τ) cross-correlation output, and are readily measured by picking the cross-correlation peaks (Berkhout and Verschuur, 2001).

In elastic media, the relationship between traveltime τ and slowness q is

$$\tau = 2zq, \quad (10)$$

where τ is the travel time between $z = 0$ and z . Slowness q , in general, varies with position (is heterogeneous) and is defined by 36 elastic coefficients C . From Taylor series, and using equation (10), the linear relationship between error ΔC in the elastic coefficients, error Δz in depth, and the travel times picked from DTS panels is

$$\Delta\tau(p) = 2q(p)\Delta z + 2z \sum_{j=1}^36 \frac{\partial \tau}{\partial C_j} \Delta C_j. \quad (11)$$

Given an analytic form for q , and an initial estimate of C_j , inversion of equation (11) yields error estimates ΔC_j that can be used to update the initial estimate.

Analytic example

For a VTI medium, quasi-P-wave-slowness q_P , and quasi-SV-wave-slowness q_{SV} , are determined by four elastic coefficients (e.g. (Kennett, 1983), p 70). In (Thomsen, 1986) notation, two of these coefficients are P-wave velocity α_0 and SV-wave velocity β_0 for $p = 0$. The remaining coefficients ϵ and δ^* are defined in terms of the elastic coefficients C_{11} , C_{33} , C_{44} , and C_{13} in (Thomsen, 1986). Note, weak anisotropy (Thomsen, 1986) is not assumed here.

For VTI media, error in traveltime $\Delta\tau$ (equation (11)) becomes

$$\Delta\tau_P(p) = 2z \left[\frac{1}{z} q_P(p) \partial_{\alpha_0} q_P(p) \partial_{\beta_0} q_P(p) \partial_{\epsilon} q_P(p) \partial_{\delta^*} q_P(p) \right] [\Delta z \Delta\alpha_0 \Delta\beta_0 \Delta\epsilon \Delta\delta^*]^T, \quad (12)$$

for P-waves and

$$\Delta\tau_{SV}(p) = 2z \left[\frac{1}{z} q_{SV}(p) \partial_{\alpha_0} q_{SV}(p) \partial_{\beta_0} q_{SV}(p) \partial_{\epsilon} q_{SV}(p) \partial_{\delta^*} q_{SV}(p) \right] [\Delta z \Delta\alpha_0 \Delta\beta_0 \Delta\epsilon \Delta\delta^*]^T,$$

for SV-waves. In the absence of SV data, as is typical in exploration seismology, converted SV-waves (PSV-waves) can be used.

When SV-wave and/or PSV-wave recordings are available, joint inversion of τ_P and τ_{SV} yields stable estimates of Δz , $\Delta\alpha_0$, $\Delta\beta_0$, $\Delta\epsilon$, and $\Delta\delta^*$ that can be used to update the initial model. That is,

$$[\alpha_0 \beta_0 \epsilon \delta^*]_{\text{new}} = [\alpha_0 \beta_0 \epsilon \delta^*]_{\text{old}} + [\Delta\alpha_0 \Delta\beta_0 \Delta\epsilon \Delta\delta^*]. \quad (14)$$

Figures 1a, 1b, and 1c show convergence curves for z and the TI parameters. In this example, the true values are $\alpha_0 = 3048 \frac{m}{s}$, $\beta_0 = 1490 \frac{m}{s}$, $\epsilon = 0.255$, and $\delta^* = -0.27$ (from (Thomsen, 1986) parameters for Shale), and thickness $z = 100m$. The values in the initial model are $\alpha_0 = 3500 \frac{m}{s}$, $\beta_0 = 1750 \frac{m}{s}$, $\epsilon = 0$, $\delta^* = 0$, and $z = 150m$.

From initial errors of magnitude 50 percent for z , 20 percent for α_0 and β_0 , and 100 percent for ϵ and δ^* , convergence to zero error occurs after ≥ 6 iterations (Figure 1a). Surprisingly, for 10 percent noise added to $\Delta\tau_P$ and $\Delta\tau_{SV}$ (Figure 1b), convergence is about the same as for zero added noise. As random noise increases to 20 percent (Figure 1c), convergence begins to require more iterations, with ϵ being the parameter most sensitive.

METHODOLOGY

Joint inversion of DTSs for P-wave and SV-waves proceeds as two

simultaneous CFP analysis procedures. Points of interest in the sub-surface are chosen as locations for analysis. Then, focusing operators, one each for P-waves and SV-waves, are computed for each analysis point by ray tracing from the surface, or by forward propagation of a modeled source. CFP gathers are computed by reverse propagation of the recorded P- and SV-wavefields to each point where each common-source gather supplies one trace to its' corresponding CFP. (As this method is based entirely on kinematics, amplitude preservation is desirable but not essential.)

The focusing operators and CFPs are transformed into the $\tau - p$ domain where they are cross-correlated. The resulting DTS panels, one for P-waves, and one for SV-waves, are analyzed for cross-correlation error. These errors are picked, and are provided as input to the joint inversion described above.

EXAMPLE

Figure 2 represents an isotropic ($\alpha = 2500 \frac{m}{s}$) medium that is 500 m thick and overlies a VTI medium ($\alpha = 3048 \frac{m}{s}$, $\beta_0 = 1490 \frac{m}{s}$, $\epsilon = 0.255$, and $\delta = -0.27$) that is 100 m thick. (These values are identical to those used in the analytic example given previously.) A point scatterer is located 490 m from the left side of Figure 2 at a depth of 600 m. Figures 3a and 3b are examples of the synthetic-shot gathers acquired for this model using a hybrid-modeling code (finite difference for isotropic layer and phase shift for the VTI layer). Figure 3a is a P-wave recording, and Figure 3b is the corresponding SV-wave recording for source locations at depth 0 m and distance 0 m.

A zero-offset section is shown in Figure 4, and a depth migration of this section is shown in Figure 5. The depth migration is parameterized using "guessed" parameters $z = 150m$, $\alpha_0 = 3500 \frac{m}{s}$, $\beta_0 = 1750 \frac{m}{s}$, $\epsilon = 0$, and $\delta^* = 0$. These erroneous values are consistent with an assumption of isotropy in the layer. That is, α_0 is over-estimated, similarly z , and a $\alpha_0/\beta_0 = 2$ is assumed. As this method is a "top-down" approach, the correct velocity is used for the isotropic overburden.

As expected, the depth to the base of the VTI layer is positioned too deep in the section at 630m (Figure 5). The diffractor, however, is quite well focused. (Error in focusing for the diffractor will probably become more apparent with greater source-receiver offset $\gg 2000$ m, as well as higher frequency $\gg 40$ Hz than is presented here.)

For CFP analysis (Berkhout and Verschuur, 2001), a common-focus (13) point is selected at the base of the VTI medium. Focusing operators (Figures 6a and 7a) are computed for this location using the "guess" parameters, and CFP gathers (Figures 6b and 7b) are similarly computed.

The focusing operators and CFP gathers are transformed into the $\tau - p$ domain (Figures 8a, 8b, 9a, and 9b) using a high-fidelity transform. The focusing-operators are then cross-correlated with the CFP gathers, and the resulting DTS panels are given in Figures 10a and 10b. Because the medium is homogeneous, DTSs $\Delta\tau_P$ and $\Delta\tau_{SV}$, indicated by starred lines on Figures 10a and 10b, are due entirely to errors in the anisotropic parameters.

In practice, $\Delta\tau_P$ and $\Delta\tau_{SV}$ are used in the joint inversion described in the previous section, and an updated model is computed. The data are re-migrated, and if the picks are reliable, the improved model yields an accurate migration result as in Figure 11. Here, the base of the VTI layer is positioned correctly at 600 m depth, and the diffractor is collapsed.

CONCLUSIONS

The joint-inversion method presented here is useful for estimating the error in thickness, and the error in the elastic parameters in anisotropic media. Based entirely on an analysis of kinematics, this method uses aspects of the well-known method of common-focal-point analysis (CFP). The differential-time shifts that arise from the CFP method are analyzed in the $\tau - p$ domain where they are related to error in vertical slowness and layer thickness. Series expansion is used to linearize this

relationship, and least-squares inversion is used to compute updates to the elastic parameters and thickness.

For stability and convergence, joint inversion makes use of quasi-P wave and quasi-SV wave data. Where SV-data are unavailable, as is most often the case in reflection seismology, we demonstrate that converted-mode-SV data (PSV) can be substituted.

Our method is found to be robust in the presence of random noise, and the analytic and synthetic examples presented demonstrate the practicality of our approach.

ACKNOWLEDGMENTS

Thanks to the Geology Foundation and the EDGER Forum at the Jackson School of Geosciences, University of Texas at Austin for supporting this work.

REFERENCES

Berkhout, A. J., and Verschuur, D. J., 2001, Seismic imaging beyond depth migration: *Geophysics*, **66**, no. 6, 1895–1912.

de Bruin, C. G. M., Wapenaar, C. P. A., and Berkhout, A. J., 1990, Angle-dependent reflectivity by means of prestack migration: *Geophysics*, **55**, no. 09, 1223–1234.

Gazdag, J., 1978, Wave equation migration with the phase-shift method: *Geophysics*, **43**, no. 07, 1342–1351.

Kabir, M. M. N., and Verschuur, D. J., 2000, A constrained parametric inversion for velocity analysis based on CFP technology: *Geophysics*, **65**, no. 4, 1210–1222.

Kennett, B. L. N., 1983, *Seismic wave propagation in stratified media*: Cambridge University Press.

Thomsen, L., 1986, Weak elastic anisotropy: *Geophysics*, **51**, no. 10, 1954–1966.

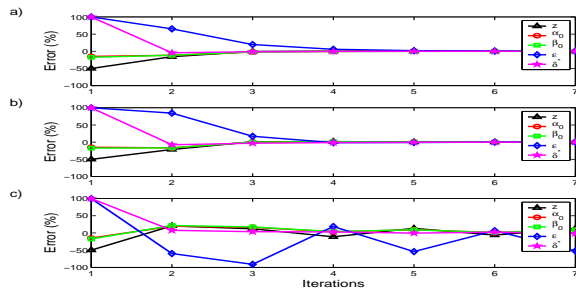


Figure 1: Convergence of the qp - qsv inversion in the presence of random noise. The true-model parameters are $\alpha_0 = 3048 \frac{m}{s}$, $\beta_0 = 1490 \frac{m}{s}$, $\epsilon = 0.255$, $\delta^* = -0.27$. The “guessed” parameters are $\alpha_0 = 3500 \frac{m}{s}$, $\beta_0 = 3500/2 \frac{m}{s}$, $\epsilon = 0$, $\delta^* = 0$. a) 0 percent random noise. b) 10 percent random noise. c) 20 percent random noise. Parameter ϵ is the most sensitive to the noise level.

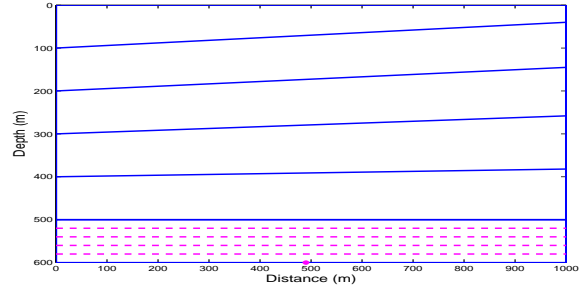


Figure 2: Geologic model. The dipping layers represent the boundaries of density contrast in an otherwise isotropic medium. Below (dashed lines), is a VTI medium with an imbedded scatterer at 600 m depth, 490 m distance. The elastic parameters of the VTI layer are the same as in Figure 1.

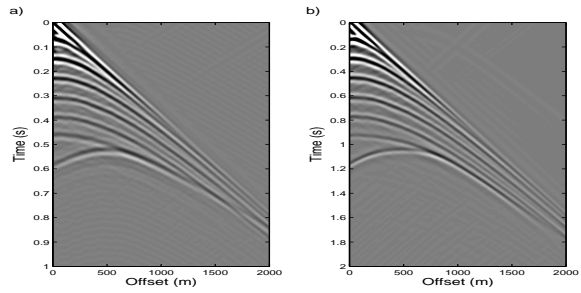


Figure 3: Synthetic-shot records corresponding to the model of Figure 2. a) P-wave (source at 0 m offset). The reflection from the base of the VTI layer is at 0.46 s at zero offset. A diffraction is centered on 500 m offset and 0.52 s. b) SV-wave (source at 0 m distance). The reflection from the base of the VTI layer is at 0.92 s at zero offset. A diffraction is centered on 500 m offset and 1.04 s.

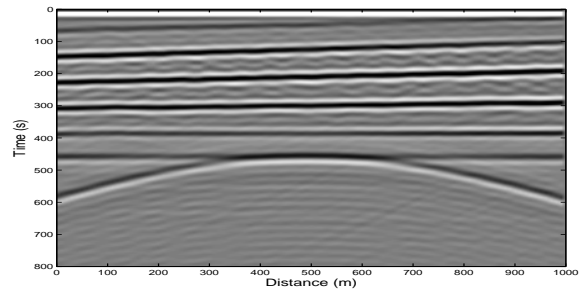


Figure 4: Synthetic-zero-offset section data corresponding to the P-wave data.

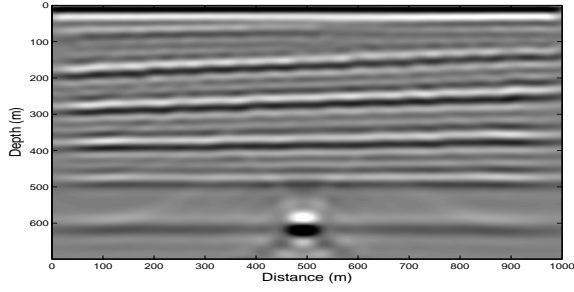


Figure 5: Depth migration of the zero-offset section of Figure 4. The correct parameters are used for the upper-isotropic section, and the "guessed" parameters ($\alpha_0 = 3500 \frac{m}{s}$, $\beta_0 = 3500/2 \frac{m}{s}$, $\epsilon = 0$, $\delta^* = 0$) are used for the VTI layer. The base of the VTI layer is imaged at 630 m instead of 600 m (Figure 2).

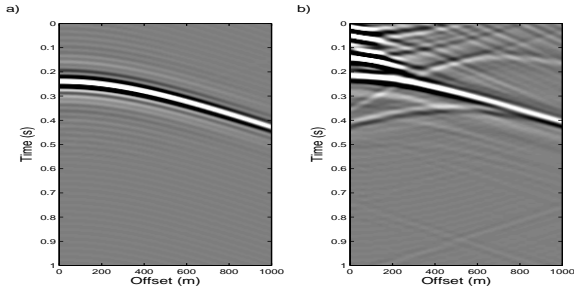


Figure 6: Focusing operator a), and CFP gather b) for P-wave data. The correct parameters are used for the upper-isotropic section, and the "guessed" parameters ($\alpha_0 = 3500 \frac{m}{s}$, $\beta_0 = 3500/2 \frac{m}{s}$, $\epsilon = 0$, $\delta^* = 0$) are used for the VTI layer.

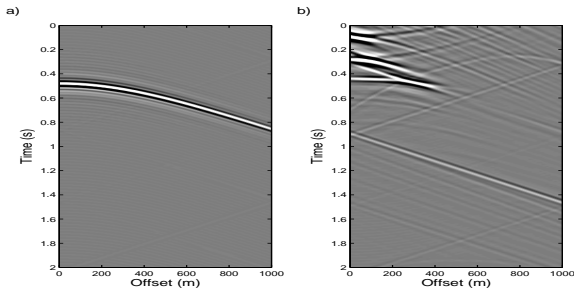


Figure 7: Focusing operator a), and CFP gather b) for SV-wave data. The correct parameters are used for the upper-isotropic section, and the "guessed" parameters ($\alpha_0 = 3500 \frac{m}{s}$, $\beta_0 = 3500/2 \frac{m}{s}$, $\epsilon = 0$, $\delta^* = 0$) are used for the VTI layer.

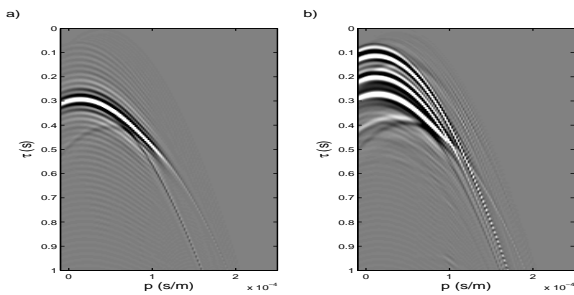


Figure 8: P-wave data in the $\tau - p$ domain. a) The focusing operator of Figure 6. b) The CFP gather of Figure 6).

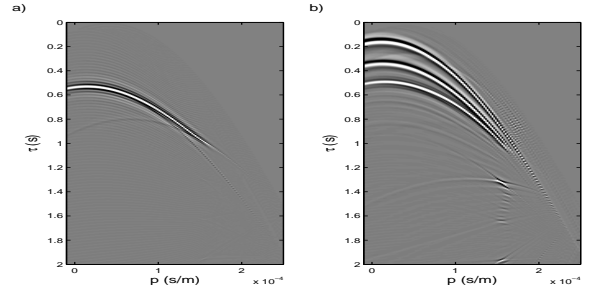


Figure 9: SV-wave data in the $\tau - p$ domain. a) The focusing operator of Figure 7. b) The CFP gather of Figure 7).

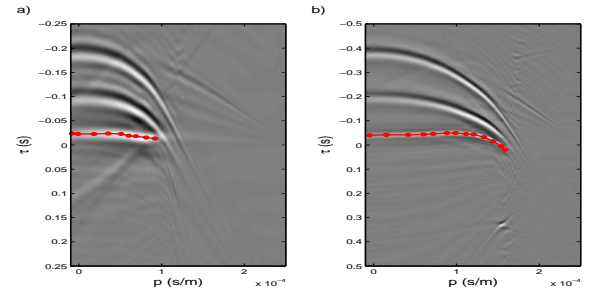


Figure 10: DTS gathers. a) P-wave. b) SV-wave. The picked events correspond to the reflections from the base of the VTI layer. The picks represent travel-time errors $\Delta\tau_p$ and $\Delta\tau_{SV}$ used the joint inversion. (For accurate model parameters, the picks lie along $\tau = 0$.)

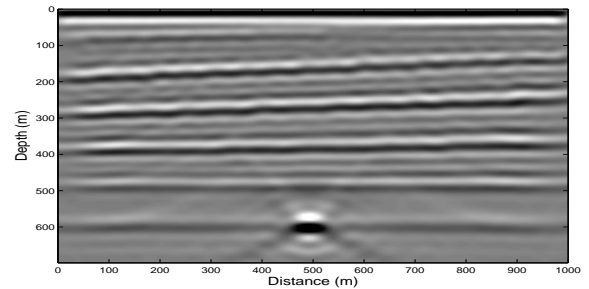


Figure 11: Final-depth migration of the zero-offset section of Figure 4. The correct parameters are used for the upper-isotropic section and the VTI layer. All layers are correctly positioned.